Nanoscale Surface Redox Chemistry Triggered by Plasmon-Generated Hot Carriers

Hao Yin, Jing-Gang Lan, Guillaume Goubert, Yao-Hui Wang, Jian-Feng Li,* and Renato Zenobi*

Direct photoexcitation of charges at a plasmonic metal hotspot produces energetic carriers that are capable of performing photocatalysis in the visible spectrum. However, the mechanisms of generation and transport of hot carriers are still not fully understood and under intense investigation because of their potential technological importance. Here, spectroscopic evidence proves that the reduction of dye molecules tethered to a Au(111) surface can be triggered by plasmonic carriers via a tunneling mechanism, which results in anomalous Raman intensity fluctuations. Tip-enhanced Raman spectroscopy (TERS) helps to correlate Raman intensity fluctuations with temperature and with properties of the molecular spacer. In combination with electrochemical surface-enhanced Raman spectroscopy, TERS results show that plasmon-induced energetic carriers can directly tunnel to the dye through the spacer. This organic spacer chemically isolates the adsorbate from the metal but does not block photo-induced redox reactions, which offers new possibilities for optimizing plasmon-induced photocatalytic systems.

1. Introduction

Photocatalysis in the visible with plasmon-induced energetic carriers (so-called hot electrons) has received significant attention.[1] Hot electrons enable a wide range of applications, e.g., water splitting,[2] ethylene epoxidation,[3] and hydrogen dissociation.[4] However, the short lifetimes of hot carriers (less than picoseconds) greatly reduces the quantum efficiency of plasmon-mediated reactions, which requires charge carriers separation followed by charge transfer to the reactants. Surface-enhanced and tip-enhanced Raman spectroscopy (SERS and TERS) are ideal analytical tools to elucidate the mechanism of plasmon-mediated reactions at the molecular level, since they provide chemical information with high sensitivity.[5] Focusing on surface molecular Raman spectroscopy, several groups have reported plasmon-mediated surface reactions, especially the coupling reaction of p-aminothiophenol (pATP).[6,7] However, because reactants are usually directly absorbed on the metal surface, the substrate could also catalyze the reaction, via different pathways. For example, in the presence of O_2, the widely studied coupling reaction of pATP on silver is thermodynamically favored and most likely triggered by adsorbed oxygen rather than by hot electrons.[8,9] One way to minimize the effect of the metal–molecule interaction is by introducing a dielectric spacer layer between the metal and the adsorbate.

The high sensitivity of SERS is mostly due to the local electromagnetic field enhancement in "hotspots" (nanoscale regions where hot electrons primarily appear[10]). Unfortunately, the enhancement in the randomly distributed hotspots on an SERS substrate can vary enormously. On the contrary, in TERS, a single metallic tip apex is used as a hotspot generator and is held in close proximity to the sample using a scanning probe microscope.[11,12] Charge carrier generation is thus limited to a single hotspot in TERS, which renders it a better spectroscopic tool for studying plasmon-mediated reactions. Here, we report how hot carriers generated under a plasmonic TERS tip can trigger reduction of Nile blue (NB) and methylene blue (MB) covalently tethered to a Au(111) surface via spacers of different length. The dyes NB and MB are used as a prototype reversible redox chromophores to study the generation and transfer of hot carriers, and the effect of temperature and spacer length. We studied the TERS signal intensity fluctuations to understand the transport mechanism of hot carriers through the spacer to the dye molecules.

H. Yin, Y.-H. Wang, Prof. J.-F. Li, Prof. R. Zenobi
MOE Key Laboratory of Spectrochemical Analysis and Instrumentation
State Key Laboratory of Physical Chemistry of Solid Surfaces
iChEM
College of Chemistry and Chemical Engineering
Xiamen University
Xiamen 361005, China
E-mail: zenobi@org.chem.ethz.ch; li@xmu.edu.cn
H. Yin, Dr. G. Goubert, Prof. R. Zenobi
Department of Chemistry and Applied Biosciences
ETH Zurich
CH-8093 Zurich, Switzerland
J.-G. Lan
Department of Chemistry
University of Zurich
CH-8057 Zurich, Switzerland

The ORCID identification number(s) for the author(s) of this article can be found under https://doi.org/10.1002/smll.201903674.

2. Results and Discussion

2.1. Chemically Bonded Dye Molecules on Au(111) Surface

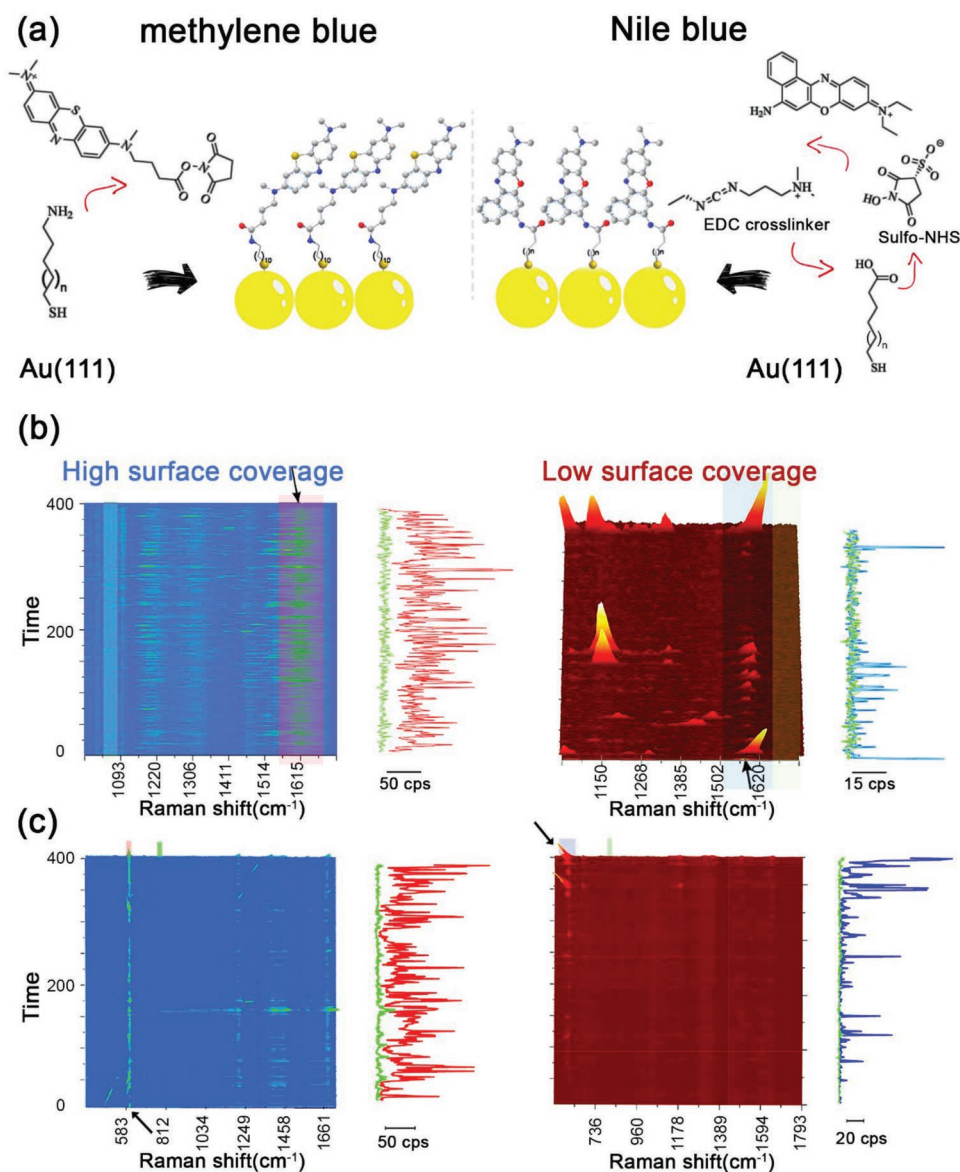The protonation of dye molecules such as MB and NB results in the formation of the corresponding leuco-dye, which have

Figure 1. a) Carbodiimide crosslinking methods used for surface molecular modification: MB (left)/NB (right). Intensity fluctuation of b) MB (≈1615 cm^{-1}) and c) NB (≈598 cm^{-1}) during TERS measurements at different surface coverages: high coverage (left) and low coverage (right). The green lines correspond to the background noise.

distinctive features in their respective UV-vis absorption spectra.[13] We used carbodiimide crosslinker chemicals to bind the dyes to the end of an alkanethiol self-assembled monolayer (SAM; **Figure 1**a). Upon binding to the surface, their molecular orbitals are mostly unperturbed by the metallic Au(111) substrate because of the insulating effect of the self-assembled thiol monolayer. The cyclic voltammograms of the covalently tethered dyes exhibit two distinct peaks, rather than one peak for physisorbed molecules[14] (Figure S1, Supporting Information). We also adjusted the density of surface functional groups in order to control the dye coverage by using a mixed thiolate SAM.[15] We chose two surface coverages: 1) full coverage of the Au surface by a single reactive thiolate SAM terminated with amino/carboxyl group (called high surface coverage below), and

2) deposition of a mixed SAM with a 1:500 ratio (20×10^{-6}:10×10^{-3} M) of reactive and nonreactive thiolates (low surface coverage). We used thiol (see the Experimental Section) to form a compact SAM layer.[16] Surface coverage measurements indicated that the number of dye molecules in the hotspot was around 1500–2000 at high coverage and 10–20 at low coverage (Figures S1 and S2 and Equation (S1), Supporting Information).

2.2. Intensity Fluctuations in TERS

In our system, a silver tip is used as a scanning tunneling microscopy (STM) probe and as an optical antenna, and Au(111) as a substrate, forming a gap mode plasmonic hotspot

with stronger field enhancement. One of our main observables was Raman intensities for MB (at 1615 cm^{-1}, Figure 1b) and NB (at 598 cm^{-1}, Figure 1c) in single point TER measurements at different surface coverages. These intensities exhibited large fluctuations, which we interpret to be due to transient reduction of dye molecules. To corroborate this interpretation, we compared this data against that from a series of common molecules with similar Raman cross-sections, but which were not affected by redox chemistry. We included nonresonant molecules and one molecule with an electronic resonance, malachite green isothiocyanate (MGITC).[17] Adsorbed MGITC on Au is less prone to undergo a redox reaction, as described by Nie and co-workers:[18] MGITC adsorbs via two different molecular moieties, the dimethylamino and isothiocyanate groups, which irreversibly locks the adsorbed molecule in its delocalized electronic structure. Upon adsorption, the central carbon atom can no longer change from sp^2 to sp^3 hybridization, which means that reduction of MGITC is inhibited. In all controls, a much more even signal intensity was found (Figure S3, Supporting Information), irrespective of the molecule's chemical structure or of the presence of an electronic resonance.

Upon reduction, the molecular electronic resonance is lost for both NB and MB, and the corresponding TERS amplitude is greatly decreased. The signal recovers spontaneously, which we interpret as reoxidation of the leuco-dyes in the presence of O$_2$ in the ambient. We propose that the interplay between plasmon-mediated reduction and spontaneous oxidation in air results in the large intensity fluctuations dominated in the TERS signal. We acquired TER spectra at low coverage to statistically analyze the proportion of the oxidized and reduced forms, where the intensity fluctuations exhibited a blinking-like (on/off) behavior. Furthermore, compared to ambient conditions, spectra characteristic of the resonant form of the dye appeared more frequently when we measured in an O$_2$-enriched atmosphere as displayed in Figure 1b,c and Figure S4 in the Supporting Information. There is a large TER intensity difference between the on and off states: when in the on state (dyes in the oxidized form) the dye fingerprint spectrum is visible; when in the off state (dyes in the reduced form) only noise is obtained because of the hundredfold weaker signal of the leuco-dye.

Blinking is also a typical phenomenon in single-molecule spectroscopy.[19a] However, the mean on- and off-times would be on the millisecond timescale for chemically tethered MB, according to Orrit's single-molecule fluorescence research.[19b] These researchers used a step-detection algorithm to extract the on- and off-times of a single chemically bonded MB molecules, which were found to follow an exponential distribution with mean on- and off-times of 10.0 ± 0.7 and 39 ± 2 ms, whereas in this study, the typical acquisition time per spectrum was 5 s. This long averaging time precludes detection of the much shorter blinking typical of single-molecule Raman experiments and averages out small fluctuations in vibrational or rotational changes in a molecule's local environment. Additionally, we expect to probe 10–20 molecules at any given time in the hotspot. We can thus safely rule out the possibility that the intensity fluctuations observed here are due to single-molecule behavior. Thermal drift of the STM tip relative to the sample is also inevitable in ambient conditions.

Drift could also cause intensity fluctuations, e.g., surface domains would cause the number of molecules within the hotspot to greatly change with pattern. To demonstrate that a uniform surface without nano-domains was formed, we used a novel probe molecule, aminomethyl benzonitrile (AMBT). AMBT was also attached to the surface using the 1-ethyl-3-(3-dimethylaminopropyl)-carbodiimide hydrochloride (EDC)/N-hydroxysulfosuccinimide (NHS) procedure (Figure S5, Supporting Information), but cannot participate in any redox reaction. Compared to the NB intensity at 598 cm^{-1} that fluctuated at low surface coverage, the TERS intensity at 1611 and 2237 cm^{-1} in the spectrum of AMBT was relatively stable, indicating the existence of a uniform substrate (**Figure 2**a,b). Therefore, we can conclude that the signal fluctuations did not result from thermal drift over a heterogenous surface.

It is challenging to obtain spectra with a high enough signal-to-noise ratio of both nonresonant leuco-dyes by TERS. We turned to SERS, which can provide a higher signal at similar conditions, to further confirm that a redox reaction takes place. As can be seen in Figure 2c, most observed Raman bands originate from the oxidized form of MB (Raman resonant). These modes were assigned with the help of qualitative density functional theory (DFT) calculations, using a relatively small basis set. Under continuous irradiation by the 633 nm laser, the intensity of the Raman peaks at 1213 and 1603 cm^{-1} increased, both stem from the reduced form of MB (leuco-MB, Figure S13, Supporting Information), while the bands of the nonreduced form of MB decreased. After stopping the laser illumination, the intensities of the 1213 and 1603 cm^{-1} bands decreased again, while bands characteristic of the oxidized dye recovered. Very likely, in the case of SERS, this is again the result of leuco-dye oxidation by O$_2$ in the air.

2.3. Hot Electron Transfer Mechanism

In our metal-SAM-dye system, carriers must pass through the thiolate SAM to trigger reduction of the dye. In other systems and experiments, charge separation and transfer were found to proceed on a fast timescale, from picoseconds[20] to microseconds.[21] The efficiency of the charge transfer strongly affects the overall quantum yield.[22–24] Aiming for further confirmation that hot electrons possess the same transfer properties as lower energy electrons,[25,26] we considered two potential charge transfer mechanisms: incoherent, thermally activated hopping, or coherent, nonresonant tunneling (**Figure 3**). The two processes have been widely discussed in the molecular electronics field,[27] suggesting that the tunneling is more distance-sensitive, while hopping is more temperature-sensitive.[28]

We investigated the hot carrier transport mechanism by comparing the occurrence of the on/off states as a function of dye-substrate distance and temperature. Since the distance from the molecular dipole of the dye to the substrate is roughly the SAM thickness, we selected two thiols with different lengths (≈0.5 nm for a 5-carbon-long chain and ≈1 nm for a 11-carbon-long chain). **Figure 4**a,b presents the electronic structures of chemically tethered MB and NB: the metal substrate has no significant influence on the lowest unoccupied molecular orbital (LUMO). To confirm that changes in the thiolate length do not
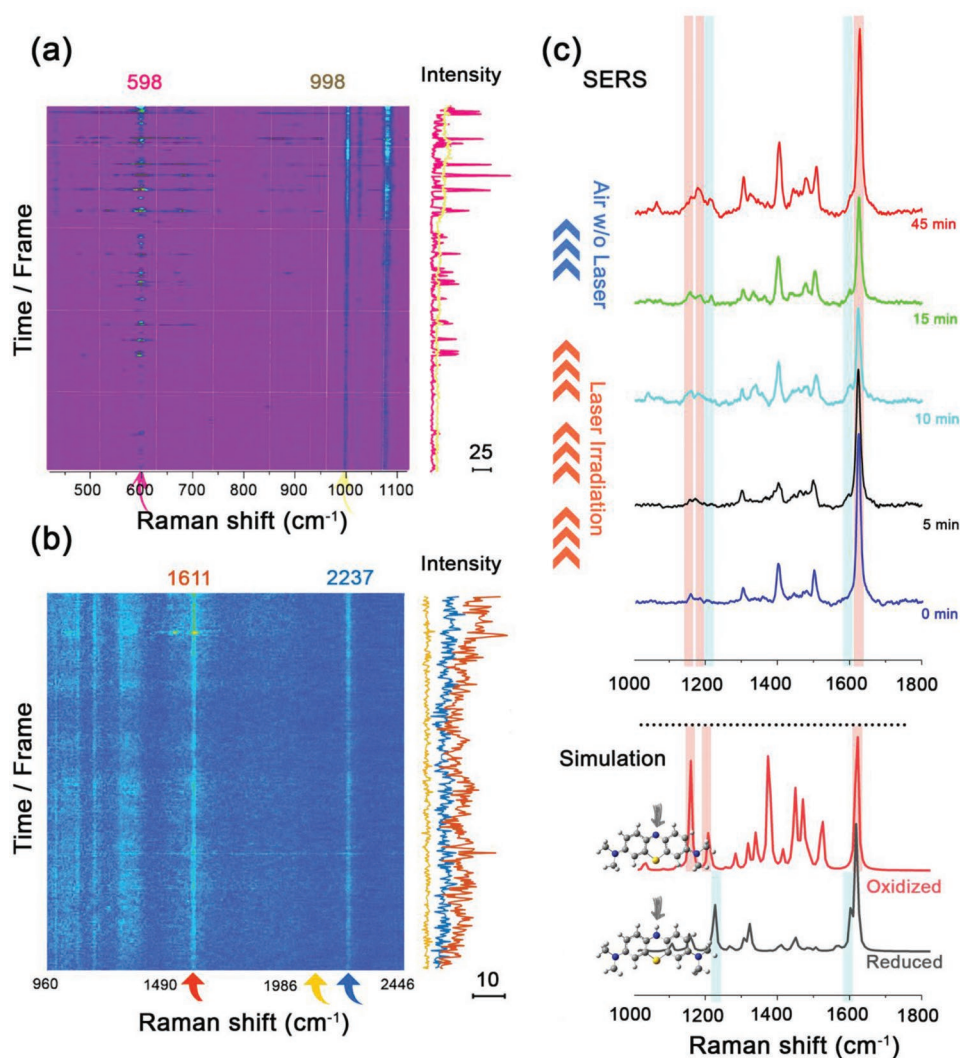
ADVANCED
SCIENCE NEWS
www.advancedsciencenews.com

NANO · MICRO
small
www.small-journal.com

Figure 2. a) TERS intensity fluctuations for NB bound to mercaptobenzoic acid/thiophenol at low surface coverage. b) TERS intensity fluctuations for (aminomethyl)benzonitrile bound to mercaptododecanoic acid/undecanethiol via the same procedure and at the same coverage. Measurement conditions: 633 nm, 0.03 mW. c) SERS experiment with MB after 633 nm laser illumination at various times, and corresponding simulation of the Raman spectra of the reduced/oxidized form.
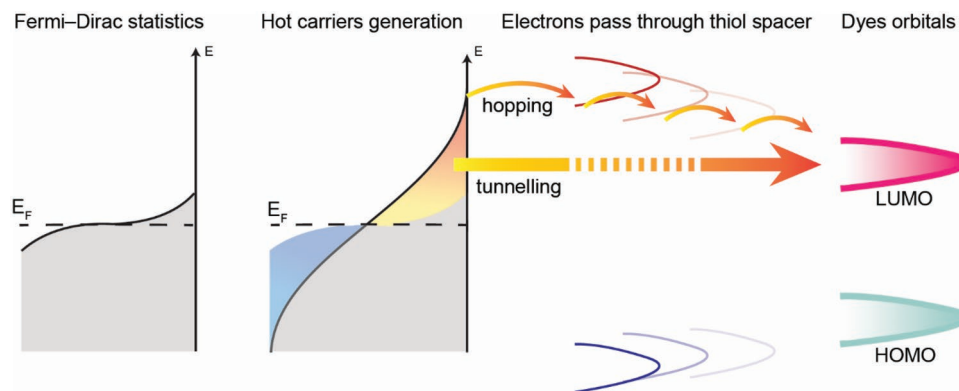

Figure 3. Potential mechanisms for generation of hot electrons and transfer to molecule orbitals. After plasmon excitation, the Landau damping and electron–electron interaction will form hot electrons that will pass through the spacers to molecular orbitals either by a tunneling or a hopping mechanism.
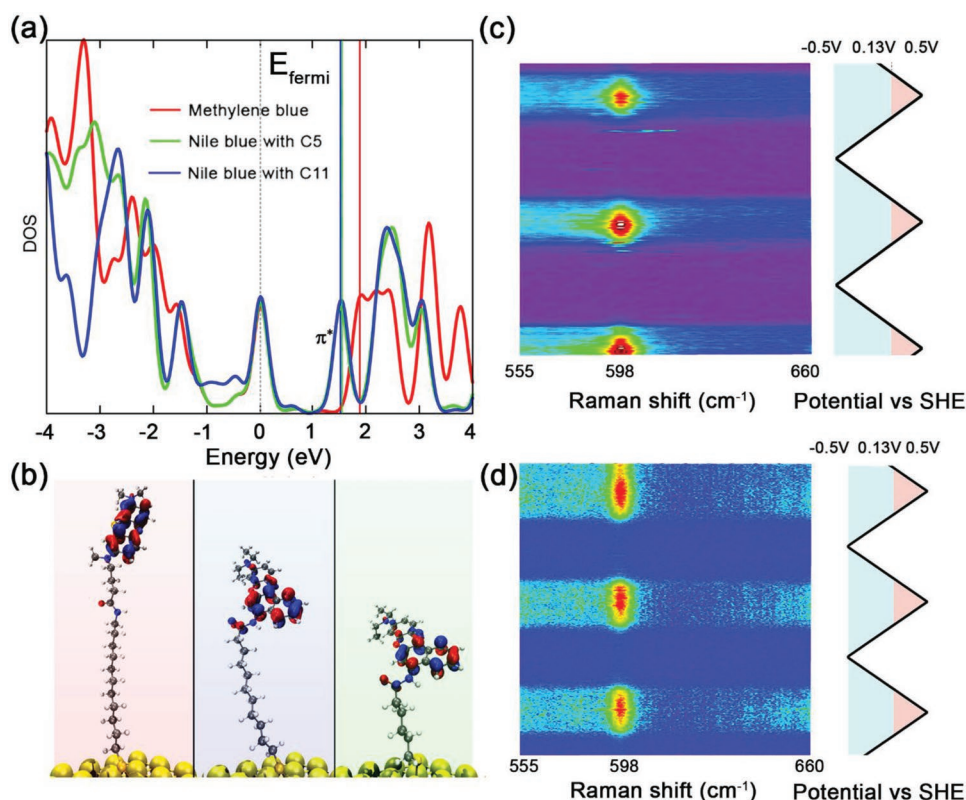
Figure 4. PDOS of the molecules adsorbed on the a) Au(111) surface and b) the corresponding isosurface of the LUMO wavefunction. EC-SERS measurements of chemically tethered NB molecules in 0.1 mol L^{-1} HClO$_4$ with the c) C5/d) C11 thiolate SAM spacers.

affect the thermodynamics of the redox reaction,[29] we measured the chemically tethered NB electrochemical (EC)-SERS signals with different thiolate spacers (Figure 4c,d). EC-SERS measurements showed a significant but reversible Raman intensity change with the potential for several cycles. The reversible redox reaction onset appeared at a similar potential, irrespective of the thiolate layer thickness.[30]

We analyzed the ratio of the oxidized to the reduced form at low surface coverage. During TERS experiments, this ratio is more than doubled, from 21% to 47%, when we chose the 1 nm thiolate spacer instead of the 0.5 nm thiolate spacer, as seen in **Figure 5**a. This change indicates that the reversible redox reaction is greatly affected by the distance between the dye and the metal surface. We then selected a longer thiolate spacer with a 15-carbon chain, surprisingly, the anomalous intensity fluctuations were not observed (Figure S6, Supporting Information) and the redox reaction did not happen as expected. We also observed a clear decrease of the Raman signal intensity and the NB fluorescence background, which was quenched with shorter spacers as shown in Figure S7 in the Supporting Information. This indicates that the metal–dye interaction was weakened and the hot electrons cannot trigger the reaction with such a long distance between the dyes and the metallic substrate. This also excludes other long-distance (more than 10 nm) energy transfer processes such as plasmon-coupled resonance energy transfer.[31a,b] We also considered a plasmonic charge transfer/tunneling mechanism which could trigger a vibrational Stark effect (as observed,

e.g., for CO,[32a] nitrile,[32b] cyanide[33c]). We selected different thiolate linkers (C5/C11) to probe the nitrile band shift of AMBT. Almost no band shift was observed (Figure S5.2, Supporting Information), which indicates that this mechanism is of minor importance in our system. To further exclude the possibility that the Ag tip generates the hot electrons for the redox reaction, we developed a wet coating method,[33] to prepare insulating silica shell-isolated tips (Figure S8, Supporting Information). The intensity fluctuations observed when using these shell-isolated tips are similar to those of bare tips (Figure S9, Supporting Information), which indicates that the hot electrons mainly originate from the Au substrate rather than from the Ag tip. This distance dependence is consistent with a tunneling mechanism where electrons transfer directly through the <1 nm thick barrier. The shorter the barrier, the higher the probability for electrons to tunnel through, which in turn leads to a higher rate for the reduction reaction. Since hopping is sensitive to the surrounding temperature, and we carried out an experiment when we maintained the substrate at different temperatures (30, 40, and 50 °C; even higher temperature may lead to the degradation of thiol-Au bonds and surface dye molecules[34]). It is also worthy to mention that, in agreement with our previous results,[35] laser-induced thermal damage of the sample did not occur under weak laser intensity (30 μW). We do not observe any signs of thermal damage from local thermal contribution,[36] such as broad carbon peaks. Figure 5b shows that the oxidized/reduced ratio varies less with temperature (22–26%) than it does with the distance (21–47%). Considering
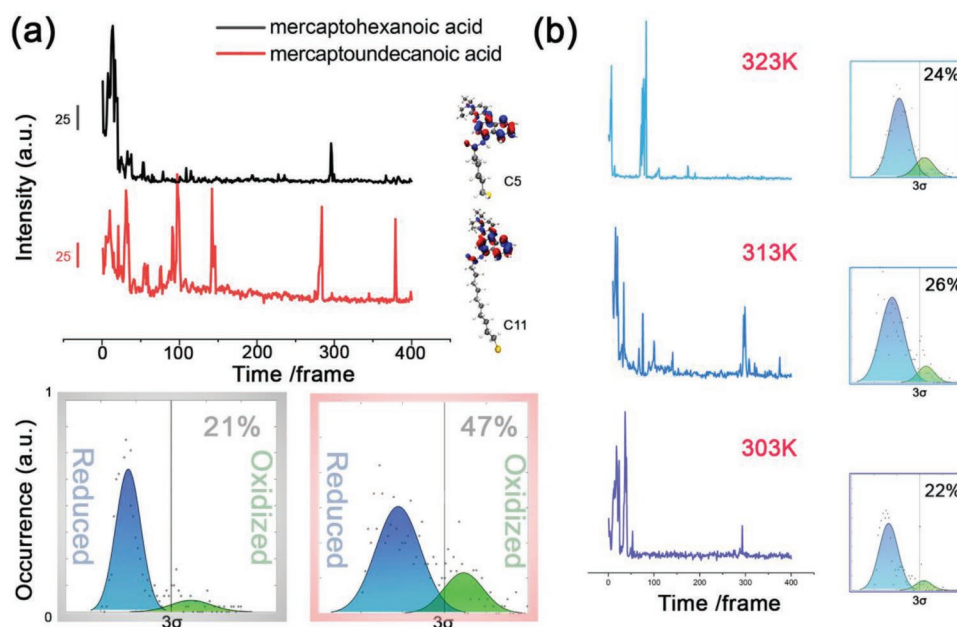
Figure 5. a) Intensity fluctuations of the 598 cm^{-1} NB TERS band and statistical analysis at low surface coverage with different thiolate spacer lengths, and b) intensity fluctuations of the 598 cm^{-1} NB TERS band and statistical analysis at low surface coverage at different temperatures. A mercaptohexanoic acid/pentanethiol layer was used in (b).

that this distance was in the sub-nm range and that the saturated alkyl chains have a poor electron affinity, we are assuming that in our dye/SAM/metal system, the charge transfer is better described by a tunneling than by a hopping mechanism which is similar to tunneling of lower energy electrons.[27]

3. Conclusions

In summary, we observed large intensity fluctuations in the Raman spectra of covalently tethered MB and NB during ambient TERS measurements, especially at low surface coverage. We found that these fluctuations result from the reduction triggered by plasmon-induced carriers in a single hotspot and spontaneous reoxidation involving ambient oxygen, which results in the reversible appearance and disappearance of the dye's resonant structure. Our study thus extends the range of plasmon-triggered reactions into surface reversible redox reactions. We also demonstrate that the transfer of energetic electrons through the donor-bridge-acceptor structure (dye/SAM/metal surface) is dominated by tunneling rather than hopping. Properties of short molecular barriers (thickness, conductivity, chemical reactivity) could be used to tune plasmon-mediated reactions. We anticipate that the new degrees of freedom that this molecular architecture provides will contribute to designing next-generation plasmonic photocatalyst with high efficiency and selectivity.

4. Experimental Section

Sample/Tip Preparation: The Au(111) single crystal bead was fabricated by Clavilier's method and was H$_2$ flame-annealed before use.

After annealing, the facets were re-located and directly fixed to a Au substrate. STM measurements were carried out with the bare Au(111) facet to show that the surface was atomically flat with a few terraces (Figure S10, Supporting Information).

The Au electrode was fabricated by directly evaporating 100 nm Au layer on glassy carbon electrode. Before the thiol treatment, a few cycles cyclic voltammetry (CV) was run in 0.1 M H$_2$SO$_4$ to clean the surface, followed by rinsing with Mill-Q water and drying under a N$_2$ atmosphere.

The silver tip was sharpened by electrochemical etching in the etching solution of perchloric acid and ethanol (1:4 v/v) under 10 V. The diameter of the apex was near 120–160 nm (Figure S11, Supporting Information). The dielectric constants of silver resulted in a larger polarizability than of gold. Besides, in gap-mode TERS, the substrate should have a strong plasmonic coupling with the tip, resulting in an extra field enhancement and a redshift of the plasmon resonance.

Assembly of Molecules on Au Surfaces: The composition of the thiol mixture should be chosen such that phase segregation into microscopic subdomains was avoided. Phase segregation was facilitated when thiols with different chain lengths were present. The energy difference was minimized by choosing thiol pairs with the same carbon chain length but different tail groups.

For thiol monolayers, the bare Au(111) substrates were immersed for 6 h in a 10×10^{-3} M ethanolic solution of one of the following compounds: phenylthiophenol (Biph), thiophenol (PhSH), MGITC, or mixed thiols to form an SAM on the surface.

For MB molecules, after modification with thiols (carrying an amino functional group) and rinsing with ethanol, the substrate was immersed into 10×10^{-3} M ethanolic MB-NHS solution for 24 h to allow the formation of chemical bond between the amino group and the NHS ester.

For NB molecules, a similar method was used, which was reported by Willets et al.[14] After modification by thiols (containing a carboxyl functional group) and rinsing with ethanol, substrates were incubated in freshly prepared 20×10^{-3} M EDC and 40×10^{-3} M NHS for 4 h. After profusely rinsing with ethanol and blowing with N$_2$, the substrate was immersed into a 10×10^{-3} M ethanoic NB solution for 24 h at room temperature to allow the formation of chemical bond between dyes and substrates.

To form a surface covered by a lower density of dyes, the substrate was immersed into a mixture of 10×10^{-3} M of a thiol without any

ADVANCED
SCIENCE NEWS

www.advancedsciencenews.com

NANO · MICRO

small

www.small-journal.com

functional group, and 20×10^{-6} M of a thiol with a functional group, for 6 h. Undecanethiol $(C_{11}H_{23}SH)$/11-amino-1-undecanethiol $(NH_2C_{11}H_{22}SH)$/12-mercaptododecanoic acid $(SHC_{11}H_{22}COOH)$, pentanethiol $(C_5H_{11}SH)$/6-mercaptohexanoic acid $(SHC_5H_{10}COOH)$, 16-mercaptohexadecanoic acid $(SHC_{15}H_{30}COOH)$/1-pentadecanethiol $(C_{15}H_{31}SH)$, as well as thiophenol/4-mercaptobenzoic acid were used for this purpose. All substrates were carefully rinsed with ethanol to remove physisorbed compounds before carrying out further experiments.

EC-SERS and Electrochemical Measurements: A PGSTAT204 modular Autolab potentiostat (Metrohm, CH) was used to conduct all electrochemical and spectrochemical measurements. For SERS measurements, a droplet was left containing 150 nm Ag nanoparticles on gold surface, then it formed coffee rings under vacuum chamber which was an ideal substrate for EC-SERS (Figure S12, Supporting Information). The measurements were operated with home-made EC-Raman cell containing of a large surface area platinum wire as counter electrode and a Calomel (Sat'd KCl) reference electrode. The scan rate 5 mV s^{-1} was used for potential control EC-SERS. The optical instrument was the same with TERS Raman spectrometer (NT-MDT, Russia, NTEGRA Spectra Upright) with 632.8 nm He-Ne laser as excitation source, an air objective (100 ×, NA = 0.7, Mitutoyo, Japan), and an electron multiplying charge-coupled device (EMCCD, Newton 971 UVB, Andor, Belfast, UK). During the measurement, 2.3 mW laser power and 2 s acquisition time were chosen to obtain significant SERS signals.

The Au(111) Electrochemical Experiment: CV was done with Pipet cell since the Au(111) facet was relatively small. The CV of Au(111) was compared in 0.1 mol L^{-1} H_2SO_4 by this method to literatures to calibrate the potential differences result from the quasi-reference electrode.

Furthermore, to measure the surface coverage, the conventional surface-analytical Au(111) electrochemistry[37] was also applied to integral the charge quantity (Figure S1, Supporting Information). The surface area was estimated by scanning electron microscope image (Figure S2, Supporting Information), and the surface average was calculated by the equilibrium equation.

TERS Measurements: The TERS instrument was described above with a combined STM module. The instrument was calibrated by a standard neon lamp (Renishaw) and Si before experiment operation. TERS maps were collected in STM feedback (constant current mode) with the sample surface be moved by the piezo sample stage in the *x*, *y*, and *z* directions while keeping the relative laser-to-tip position fixed. An exposure time of 5 s was used for all spectra. The HeNe laser was set at an incident power of 30 µW in order to avoid the photo-bleaching and thermal damaging on the surface of nano-antennas.[17,34] During TERS measurements, the bias voltage was set to 0.3 V (to prevent bias triggered reaction),[38,39] and the tunneling current was kept at 0.2 nA to avoid scratching the sheet. All TERS images were obtained after overnight measurements to minimize the thermal drift of the system.

Data Analysis and Calculations: Analysis method: All spectra shown in this work had been processed by the following methods: background subtraction, Savitzky–Golay smoothing, cosmic ray removal. For significance analysis for low surface intensity, the signals above 3 standard deviation ($3\sigma1$) of noise level were considered valid-resonant for further statics for each spectrum. Normal distribution was applied for each region and the intensity (*x*-axis) was rescaled for visualization. All the data were analyzed with Matlab_R2017b software with build-in packages.

Noise floor was determined for NB and MB. A region was chosen with blank Raman peak and close to the target band as noise floor. The mean value of noise floor was taken to further analyze (Mnoise). Since the fluctuation could also result from the instable laser intensity, the standard deviation $\sigma2$ of Mnoise was calculated corresponding to time. Only the signals above of $3\sigma2$ were resulted from redox reaction instead of laser fluctuation. It was assumed that the nonresonance structure/resonance Raman intensity would obey normal distribution separately and the integration of the total probability density function was set to be 1. The data were analyzed first to point out the typical noise region to fit normal distribution and the corresponding sigmaHat was calculated. The data above $3\sigma2$ were assigned as the valid resonance signals to fit another normal distribution, the final data were normalized

by the ratio of their highest peak (also the ratio in Figure S4, Supporting Information).

Calculation Methods: Raman spectra of free molecules were calculated with Gaussian 09. The basis sets for C, N, S, O, and H atoms were 6–31+G*. Full geometry optimizations and frequency analyses were carried out by using Gaussian 09 package. To understand the vibrational spectra of MB, a scaling factor of 0.978 was used for the vibrational frequencies related to the internal coordinators to the force constant matrix calculated at the B3LYP/6–31+G* level. This moderate level of theory already helped a lot to understand the appearance of bands characteristic of the reduced form.

The metal slab was consisted of four (6 × 6) gold (111) atomic layers. The molecules were linked via Au-S bond and their LUMO are plotted accordingly in Figure 4. All the simulations were carried out by keeping the two bottom Au layers fixed at the initial coordinates in order to maintain the bulk behavior of the inner part of the slab. DFT calculation was performed by using the CP2K package, Perdew–Burke–Ernzerhof functional with Grimme D3 correction was used to describe the system. Unrestricted Kohn–Sham DFT had been used as the electronic structure method in the framework of the Gaussian and plane waves method. The Goedecker–Teter–Hutter (GTH) pseudopotentials, DZVP-MOLOPT-GTH basis sets were utilized to describe the molecules. A plane-wave energy cut-off of 500 Ry had been employed. The electronic structure analysis was carried out in terms of the projected density of state (PDOS) of the molecules adsorbed on the Au(111) surface.

Supporting Information

Supporting Information is available from the Wiley Online Library or from the author. The original data used in this publication are made available in a curated data archive at ETH Zurich (https://www.research-collection.ethz.ch) under the https://doi.org/10.3929/ethz-b-000367674.

Conflict of Interest

The authors declare no conflict of interest.

[1] M. L. Brongersma, N. J. Halas, P. Nordlander, *Nat. Nanotechnol.* **2015**, *10*, 25.

[2] S. Mubeen, J. Lee, N. Singh, S. Kramer, G. D. Stucky, M. Moskovits, *Nat. Nanotechnol.* **2013**, *8*, 247.

[3] S. Linic, P. Christopher, D. B. Ingram, *Nat. Mater.* **2011**, *10*, 911.

[4] S. Mukherjee, F. Libisch, N. Large, O. Neumann, L. V. Brown, J. Cheng, J. B. Lassiter; E. A. Carter, P. Nordlander, N. J. Halas, *Nano Lett.* **2013**, *13*, 240.

[5] B. de Nijs, F. Benz, S. J. Barrow, D. O. Sigle, R. Chikkaraddy, A. Palma, C. Carnegie, M. Kamp, R. Sundararaman, P. Narang, O. A. Scherman, J. Baumberg, *Nat. Commun.* **2017**, *8*, 994.

[6] Y. F. Huang, M. Zhang, L. B. Zhao, J. M. Feng, D. Y. Wu, B. Ren, Z. Q. Tian, *Angew. Chem., Int. Ed.* **2014**, *53*, 2353.

[7] E. M. van Schrojenstein Lantman, T. Deckert-Gaudig, A. J. Mank, V. Deckert, B. M. Weckhuysen, *Nat. Nanotechnol.* **2012**, *7*, 583.

[8] L. B. Zhao, M. Zhang, Y. F. Huang, C. T. Williams, D. Y. Wu, B. Ren, Z. Q. Tian, *J. Phys. Chem. Lett.* **2014**, *5*, 1259.

[9] A. da Silva, T. Rodrigues, V. Correia, T. Alves, R. Alves, R. Ando, F. Ornellas, J. Wang, L. Andrade, H. Camargo, *Angew. Chem., Int. Ed.* **2016**, *55*, 7111.

[10] E. Cortés, W. Xie, J. Cambiasso, A. S. Jermyn, R. Sundararaman, P. Narang, S. Schlücker, S. A. Maier, *Nat. Commun.* **2017**, *8*, 14880.

[11] J. H. Zhong, X. Jin, L. Meng, X. Wang, H. S. Su, Z. L. Yang, C. T. Williams, B. Ren, *Nat. Nanotechnol.* **2016**, *12*, 132.

[12] R. Zhang, Y. Zhang, Z. C. Dong, S. Jiang, C. Zhang, L. G. Chen, L. Zhang, Y. Liao, J. Aizpurua, Y. Luo, J. L. Yang, J. G. Hou, *Nature* **2013**, *498*, 82.

[13] D. Kurouski, M. Mattei, R. P. van Duyne, *Nano Lett.* **2015**, *15*, 7956.

[14] A. J. Wilson, N. Y. Molina, K. A. Willets, *J. Phys. Chem. C* **2016**, *120*, 21091.

[15] C. D. Bain, E. B. Troughton, Y. T. Tao, J. Evall, G. M. Whitesides, R. G. Nuzzo, *J. Am. Chem. Soc.* **1989**, *111*, 321.

[16] C. Vericat, M. E. Vela, G. Benitez, P. Carro, R. C. Salvarezza, *Chem. Soc. Rev.* **2010**, *39*, 1805.

[17] B. Pettinger, B. Ren, G. Picardi, R. Schuster, G. Ertl, *J. Raman Spectrosc.* **2005**, *36*, 541.

[18] X. Qian, S. R. Emory, S. Nie, *J. Am. Chem. Soc.* **2012**, *134*, 2000.

[19] a) S. Nie, S. R. Emory, *Science* **1997**, *275*, 1102. b) W. Zhang, M. Caldarola, B. Pradhan, M. Orrit, *Angew. Chem., Int. Ed.* **2017**, *56*, 3566.

[20] K. Wu, J. Chen, J. R. McBride, T. Lian, *Science* **2015**, *349*, 632.

[21] D. P. dos Santos, M. L. A. Temperini, A. G. Brolo, *J. Am. Chem. Soc.* **2012**, *134*, 13492.

[22] B. Foerster, A. Joplin, K. Kaefer, S. Celiksoy, S. Link, C. Sönnichsen, *ACS Nano* **2017**, *11*, 2886.

[23] Y. Zhang, S. He, W. Guo, Y. Hu, J. Huang, J. R. Mulcahy, W. D. Wei, *Chem. Rev.* **2018**, *118*, 2927.

[24] J. R. M. Saavedra, A. Asenjo-Garcia, F. J. Garcia de Abajo, *ACS Photonics* **2016**, *3*, 1637.

[25] a) Y. Kim, A. J. Wilson, P. K. Jain, *ACS Catal.* **2017**, *7*, 4360. b) E. Fung, O. Adak, G. Lovat, D. Scarabelli, L. Venkataraman, *Nano Lett.* **2017**, *17*, 1255.

[26] C. E. D. Chidsey, *Science* **1991**, *251*, 919.

[27] S. H. Choi, B. Kim, C. D. Frisbie, *Science* **2008**, *320*, 1482.

[28] M. A. Reed, C. Zhou, M. R. Deshpande, C. J. Muller, T. P. Burgin, L. Jones II, J. M. Tour, *Ann. N. Y. Acad. Sci.* **1998**, *852*, 133.

[29] R. P. Gautam, Y. T. Lee, G. L. Herman, C. M. Moreno, E. C. M. Tse, C. J. Barile, *Angew. Chem., Int. Ed.* **2018**, *57*, 13480.

[30] A. J. Wilson, K. A. Willets, *Analyst* **2016**, *141*, 5144.

[31] a) J. Li, S. K. Cushing, F. Meng, T. R. Senty, A. D. Bristow, N. Wu, *Nat. Photonics* **2015**, *9*, 601. b) L. Y. Hsu, W. Ding, G. C. Schatz, *J. Phys. Chem. Lett.* **2017**, *8*, 2357.

[32] a) M. Banik, P. Z. El-Khoury, A. Nag, A. Rodriguez-Perez, N. Guarrottxena, G. C. Bazan, V. A. Apkarian, *ACS Nano* **2012**, *6*, 10343. b) D. A. Nelson, Z. D. Schultz, *J. Phys. Chem. C* **2019**, *123*, 20639. c) J. M. Marr, Z. D. Schultz, *J. Phys. Chem. Lett.* **2013**, *4*, 3268.

[33] L. Opilik, Ü. Dogan, C. Li, B. Stephanidis, J. Li, R. Zenobi, *J. Phys. Chem. C* **2016**, *120*, 20828.

[34] T. E. Tesema, B. Kafle, M. G. Tadesse, T. G. Habteyes, *J. Phys. Chem. C* **2017**, *121*, 7421.

[35] J. Szczerbiński, L. Gyr, J. Kaeslin, R. Zenobi, *Nano Lett.* **2018**, *18*, 6740.

[36] L. Zhou, F. D. Swearer, C. Zhang, H. Robatjazi, H. Zhao, L. Henderson, L. Dong, P. Christopher, E. Carter, P. Nordlander, N. Halas, *Science* **2018**, *362*, 69.

[37] M. J. Esplandiu, H. Hagenström, D. M. Kolb, *Langmuir* **2001**, *17*, 828.

[38] H. Bi, C. Palma, Y. Gong, P. Hasch, M. Elbing, M. Mayor, J. Reichert, V. J. Barth, *J. Am. Chem. Soc.* **2018**, *140*, 4835.

[39] S. Fatayer, B. Schuler, W. Steurer, I. Scivetti, J. Repp, L. Gross, M. Persson, G. Meyer, *Nat. Nanotechnol.* **2018**, *3*, 376.

1903674 (8 of 8)